



Acoustic-driven droplet evaporation: beyond the role of droplet-gas relative velocity



Avshalom Offner^{a,1}, Nir Berdugo^{b,1}, Dan Liberzon^{c,*}

^a School of Mathematics, The University of Edinburgh, Edinburgh EH9 3FD, United Kingdom

^b Interdisciplinary Graduate Program for Applied Mathematics, Technion – Israel Institute of Technology, Haifa 32000 Israel

^c Interdisciplinary Graduate Program for Applied Mathematics and Faculty of Civil & Environmental Engineering, Technion – Israel Institute of Technology, Haifa 32000, Israel

ARTICLE INFO

Article history:

Received 7 November 2020

Revised 27 January 2021

Accepted 5 February 2021

2010 MSC:

00-01

99-00

Keywords:

elsarticle.cls

LaTeX

Elsevier

template

ABSTRACT

Acoustic waves can be used for high-precision evaporation of droplets, allowing for fine control over the droplet diameter. Previous works considered the acoustic field as simply a means for generating relative velocity u_1 between a droplet and its surrounding gas, which convects heat and mass from the droplet while oscillating. In the present work, we experimentally examine the effects of an acoustic field fundamental characteristics – pressure and velocity distribution and the phase between them – on a droplet evaporation rate. Our results clearly show that the pressure and phase contribute to the evaporation, with the latter dramatically affecting the process. We propose a generalization to existing models that account only for variations in u_1 , and demonstrate how the new model outperforms its counterpart when fitted to the experimental data. Our generalized correlation increases R^2 for fitting the experimental data from 0.82 to 0.94, when compared with a standard model that only accounts for relative velocity. The new insight may be utilized for enhancement and fine-tuned control over droplet evaporation via acoustics, to be used over a wide range of applications, including lab-on-a-droplet reactions and vapor transport in thermoacoustic devices.

© 2021 Elsevier Ltd. All rights reserved.

1. Introduction

Acoustics is commonly used to enhance and control evaporation of droplets in a gaseous environment. Such processes are key in a variety of fields, including drying sprays in agricultural [1] or pharmaceutical [2] applications, fine-tuned control over a droplet water content in protein reactions [3,4], and the use of mist for vapor transport by thermoacoustic devices [5,6]. Acoustic-driven evaporation of sub-mm droplets may be classified into high and low frequency regimes, governed by different physical mechanisms and distinguished by the *Strouhal* number, $St = fR/u_1 \propto R/\xi_1$, where f is the acoustic frequency, R is the droplet radius and u_1 and $\xi_1 \propto u_1/f$ are the oscillating gas velocity and displacement, respectively. At high frequencies ($St > 1$), high-intensity acoustic waves vibrate the droplet and enhance its vaporization by increasing its temperature [7–12]. At low frequencies ($St \ll 1$), the gas displacement ξ_1 is much larger than the droplet radius and the acoustic field enhances the evaporation by flowing low-vapor-pressure gas

over the droplet surface. The latter utilizes exergy from the surrounding gas and therefore constitutes an energy-efficient method for droplet evaporation [13–18].

The enhancement in droplet evaporation rate by presence of a low-frequency acoustic field is traditionally associated only with the imposed non-zero relative velocity between the droplet and gas [14–16]. However, additional inherent features of an acoustic field may also contribute to the evaporation. The oscillatory pressure field around a droplet induces momentary deviations in the gas vapor pressure, thus periodically increasing the vapor-pressure difference between the droplet and gas and subsequently enhance the evaporation rate. Furthermore, the phase angle between the oscillating pressure and velocity fields can dramatically affect the evaporation, synchronizing between the vapor release from the droplet and the gas velocity that carries it away from the source. While the interplay between pressure and velocity largely impacts the performance and efficiency of acoustic systems, to the best of our knowledge no studies examined how this interplay affects the evaporation of droplets in an acoustic field. In the present work, we experimentally examine how characteristic properties of the standing wave acoustic field enhance the droplet evaporation rate, and derive a simple model to quantify the relative contribution of each property to the overall effect.

* Corresponding author.

E-mail address: liberzon@technion.ac.il (D. Liberzon).

¹ Equal Contributors

Nomenclature

A	Droplet surface area (m^2)
c	Minimization parameter
DR	Drive ratio
f	Resonance frequency (Hz)
\bar{h}	Averaged heat transfer coefficient ($\text{W m}^{-2} \text{K}^{-1}$)
h_{fg}	Latent heat of evaporation (J kg^{-1})
H	Relative humidity
L	Spheroidal droplet long radius (m)
p	Pressure (Pa)
P	Scaled pressure oscillation amplitude
r	Cylinder outer radius (m)
R	Spherical droplet radius/Spheroidal droplet short radius (m)
Re	Reynolds number
St	Strouhal number
t	Time (s)
T	Temperature (K)
ΔT	Droplet-gas temperature difference (K)
u	Droplet-gas relative velocity (m/s)
X	Scaled position within the resonator

Greek symbols

α	Minimization parameter
β	Minimization parameter
γ	Minimization parameter
ϕ	Pressure-velocity phase lag
θ	Phase lag deviation from standing wave
ξ	Droplet-gas relative displacement (m)

Subscripts and accents

1	Oscillating
m	Time-averaged
max	Maximal
$N.A$	No acoustics
$\hat{\quad}$	Dimensionless

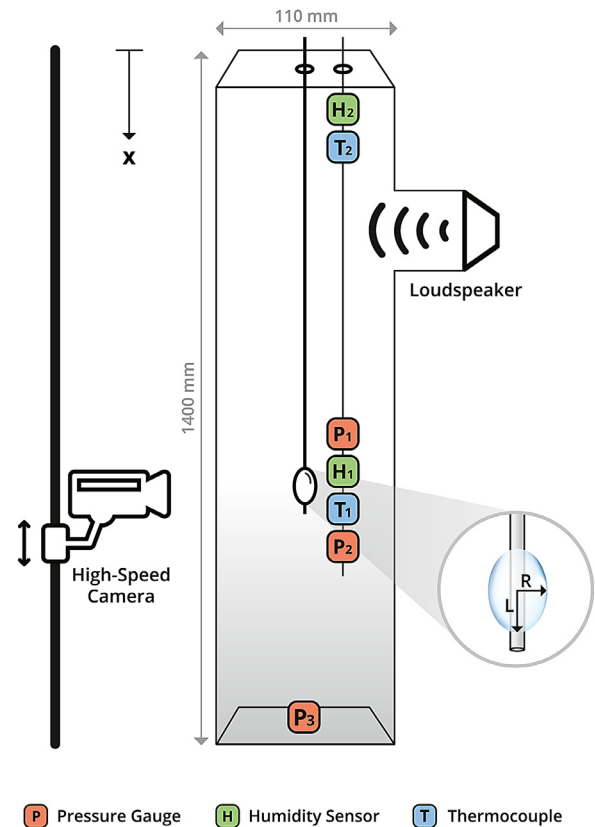


Fig. 1. Experimental setup schematic drawing. The droplet attaches to the outer surface of a thin glass-filament-tube through which it is introduced. A close view of the droplet shows its spheroid shape, specifying its radii R and $L > R$. A thin rod, aligned with the thin tube, carries measurement devices that monitor pressure, humidity and temperature near the droplet and at the resonator upper surface. An additional pressure gauge monitors the maximal pressure amplitude at the resonator floor. A loudspeaker drives acoustic oscillations at the system first resonant mode ($f = 115$ Hz), thus enhancing the droplet evaporation rate. The evaporation process is recorded by a high-speed camera at 500 frames per second.

2. Experimental setup

To examine the evaporation rate of a single, pending droplet in an acoustic field under varying conditions, an experimental setup was designed and fabricated. The setup consisted of a standing-wave acoustic resonator, namely a vertically-oriented closed duct with square cross-section, made of transparent acrylic (see Fig. 1). Near the resonator upper surface, a tee junction with a side branch was installed, housing a loud-speaker (Cerwin Vega U84dD), driven by a signal generator and an amplifier (Samson Servo 120a), which generated a monochromatic, standing acoustic wave at the system first resonant mode of $f = 115$ Hz. A long, rigid rod was inserted through the center of the resonator upper surface, carrying a hair-thin glass-filament tube ($80 \mu\text{m}$ in diameter) that was used to generate a pending droplet with radius $R \sim 300 - 350 \mu\text{m}$ via the following methodology. Distilled deionised Water at $25 \pm 2^\circ \text{C}$ was introduced through the thin tube using a syringe, producing a hanging droplet, $\sim 800 \mu\text{m}$ in diameter. The syringe was then pulled, applying negative pressure to pump excessive water from the tube. Most of the droplet mass did not flow back into the thin tube, but rather soared and adhered to the thin tube outer surface due to the asymmetric shape of the tube opening, creating a spheroid-like droplet, $550 - 800 \mu\text{m}$ in diameter. The droplet position along the resonator main axis was adjusted by sliding the rod to enable testing of droplet evaporation at various positions within the acoustic field. A second rod was inserted alongside the first, equipped with two pressure gauges (Evdevco 8510-b, accuracy ± 0.05 Pa at sam-

pling rate 2 kHz), a K-type thermocouple (accuracy ± 0.1 K) and a humidity sensor (Rotronic H2C-IE302, accuracy $\pm 1\%$). The acoustic pressure oscillation amplitude p_1 , the temperature T and the relative humidity H near the vaporizing droplet were measured directly. The velocity u_1 was evaluated from two closely located pressure measurements and their respective phase difference ϕ , using the two-microphone method, accurate to within 5% [19]. A third pressure gauge was located on the resonator bottom to record the highest pressure amplitude in the system, from which the drive ratio $DR \equiv p_{max}/p_m$ is calculated, where $p_m \approx 1$ bar is the mean pressure measured in the resonator throughout the experiments. The temperature and relative humidity were also monitored at the resonator upper end to reflect the system reference conditions. The droplet evaporation process was recorded by filming a 3×3 mm field of view, in which the resolution was $5.8 \mu\text{m}/\text{pixel}$, using a high-speed camera (Ametek MIRO 310) at 500 frames per second, approximately 4.5 times faster than the acoustic-oscillation cycle (see supplementary videos 1 and 2 for a representative experiment footage).

3. Experimental procedure

The overarching goal of this set of experiments was to examine whether organic features of an acoustic field that were previously neglected – p_1 and ϕ – affect the droplet evaporation rate. Since velocity and pressure are coupled in an acoustic field, exper-

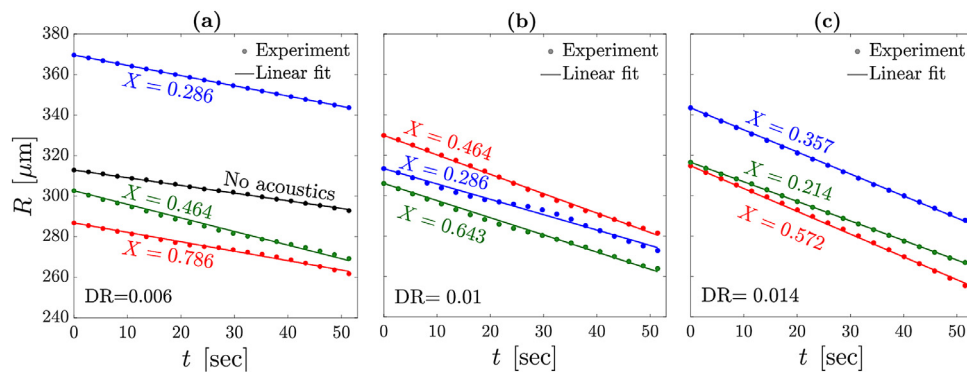


Fig. 2. Time-series measurements of the droplet radius $R(t)$ at various dimensionless positions $0 \leq X \leq 1$, with $X = 0$ marking the resonator upper surface, for (a) $DR = 0.006$ (no acoustics result drawn for reference), (b) $DR = 0.01$ and (c) $DR = 0.014$. Filled dots represent experimental measurements and the lines are least-squares fit to the data set from each experiment.

iments were run with two varying parameters to isolate the effects of p_1 and ϕ from that of relative velocity between the (immobilized) droplet and gas. Experiments were conducted at 3 loudspeaker volumes (thereafter quantified as DR values), accounting for a mutual increase/decrease in both pressure and velocity near the droplet. At each DR, measurements at 7 droplet positions along the resonator were conducted, in which a shift in position leads to an increase in pressure and a decrease in velocity, or vice versa. Including experiments performed in the absence of acoustics, a total of 28 unique experimental conditions were examined. All experiments were run for 55 seconds, so as to allow sufficient time for significant decrease to the droplet radius R all the while avoiding extreme variations as $R \rightarrow 0$.

The resonator was flushed with dry air prior to each experiment to ensure the initial conditions are maintained nearly identical. Flushing terminated when the temperature and humidity measurements read $25 \pm 2^\circ\text{C}$ and $15 \pm 1.5\%$, respectively. To ensure reproducibility, three repetitions were conducted at all experimental conditions. The standard deviation from the mean for each set of repetitions did not exceed 4.5% of the respective mean value. Camera recordings from each experiment were broken into a series of 8-bit images on which image analysis was performed to extract time series for the droplet geometry variations during evaporation.

4. Results and discussion

Representative experimental measurements of the droplet radius $R(t)$ are presented in Fig. 2, showing three experiments conducted at different positions along the resonator for each DR. $0 \leq X \leq 1$ marks the scaled position along the resonator with $X = 0$ denoting the resonator upper surface. The results clearly show a linear trend in $R(t)$, illustrated by the linear regression fitted to the data. Results form a single, representative experiment with no acoustics are drawn in Fig. 2a for reference, so as to demonstrate that these conditions also recover a linear trend with a noticeably restrained slope.

Since the droplet in our experiments adhered to the outer surface of the thin tube by surface tension, its shape resembled a prolate spheroid with radii R and L , through which a cylinder of outer radius r cuts along its axis (see Fig. 1 and supplementary video). In Fig. 3a we show a representative example of the diminution of both radii during an experiment (for $X = 0.572$ and $DR = 0.006$). The data are scaled with $R_0 \equiv R(t = 0)$ to quantitatively demonstrate that the difference between the radii is very small, i.e. $\varepsilon = (L - R)/R_0 \approx 0.1 \ll 1$. The results clearly show that both radii decreased linearly; the lowest value for the coefficient of determination throughout the measurements was $R^2 = 0.97$. Additionally, both radii decrease linearly with a nearly identical slope. To illus-

trate this further, we calculated time derivatives for $R(t)$ and $\varepsilon(t)$ using forward differences, the results of which are presented in Fig. 3b. In scaled form, it is straightforward that $|\text{d}\varepsilon/\text{d}t| \ll |\text{d}R/\text{d}t|$, such that ε may be safely approximated as a constant.

4.1. Theoretical model

To model the droplet evaporation process, we employed a simple energy balance, assuming that convection is the sole mechanism by which heat is transferred to the droplet that evaporates, hence

$$\frac{\text{d}}{\text{d}t}(\rho V h_{fg}) = -\bar{h} A \Delta T, \quad (1)$$

where ρ is the liquid droplet density, V is the droplet volume, h_{fg} is the heat of vaporization, t is time, \bar{h} is the average convective-heat-transfer coefficient, A is the droplet surface area and $\Delta T \equiv T_g - T_d > 0$ is the temperature difference between the gas and the droplet. Heat conduction between the droplet and glass tube was neglected in the model, since the narrow cylindrical surface is much smaller than the droplet surface, exposed to convection. ρ and h_{fg} are generally a function of the droplet temperature $T_d(t)$. While T_d itself varies only little, the dependency of ρ and h_{fg} on the temperature is also weak and therefore we treat them as constants. Accordingly, Eq. (1) simplifies to

$$\Lambda = -\frac{\bar{h} \Delta T}{\rho h_{fg}}, \quad (2)$$

where

$$\Lambda \equiv \frac{1}{A} \frac{\text{d}V}{\text{d}t} \quad (3)$$

is defined for convenience. For a spherical droplet $\Lambda = \text{d}R/\text{d}t$, such that Eq. (2) simplifies to

$$\frac{\text{d}R}{\text{d}t} \approx -\frac{\bar{h} \Delta T}{\rho h_{fg}}. \quad (4)$$

The right side of Eq. (4) is generally time-dependent, however variations in ΔT are typically small and may therefore be neglected with no considerable loss of accuracy. The heat-transfer coefficient \bar{h} generally depends on $R(t)$; a common model for this dependency is $\bar{h} \propto R^{-1}$, yielding the well known Spalding law [20]. However, since here $R^{-1} \text{d}R/\text{d}t$ is small, namely the droplet radius does not approach zero and the diminution rate is relatively moderate, \bar{h} may be treated as a constant over relatively short periods of time, while the droplet radius does not yet appreciably decrease. This reveals that $\text{d}R/\text{d}t \approx \text{const.}$, in agreement with the experimental observations in Fig. 2.

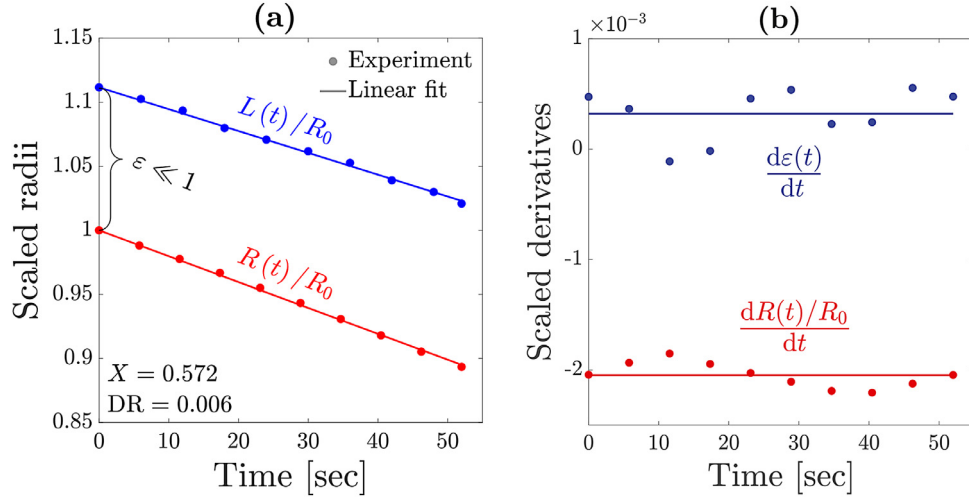


Fig. 3. (a) Representative time-series measurements of the spheroid droplet primary radii $R(t)$ and $L(t)$, scaled by the droplet initial radius $R_0 \equiv R(t=0)$. Filled dots represent experimental measurements and the lines are least-squares fit to the data. The parameter $\varepsilon = (L - R)/R_0 \approx 0.1$ satisfies the assumption $\varepsilon \ll 1$, used in § 4.1. (b) Time derivatives for R and ε , calculated using finite differences. Solid lines represent the respective means for each set of data. The data reveal that $|d\varepsilon/dt| \ll |d\hat{R}/dt|$, where $\hat{R} = R/R_0$.

As indicated earlier, the droplet in our experiments deviated from a perfectly spherical shape. In what follows, we show that this result is recovered for weakly-spheroidal droplets through an asymptotic analysis. The volume and surface area of a prolate spheroid through which a cylinder of radius r cuts along the axis, are

$$V = \frac{4}{3}\pi R^2 L - 2L\pi r^2, \quad (5)$$

$$A = 2\pi R^2 \left(1 + \frac{L}{R} \frac{\arcsin e}{e}\right) - 2\pi r^2, \quad e^2 = 1 - \left(\frac{R}{L}\right)^2. \quad (6)$$

We scale the variables as follows

$$R = R_0 \hat{R}, \quad L = R_0 \hat{L}, \quad r = R_0 \hat{r}, \quad V = 4\pi R_0^3 \hat{V}, \quad A = 4\pi R_0^2 \hat{A}, \quad t = \omega^{-1} \hat{t}, \quad \Lambda = R\omega \hat{\Lambda} \quad (7)$$

in which a hat sign marks a dimensionless quantity and the scaling for V and A were chosen such that the scaled form of Λ remains unchanged. Next, we rewrite 5-(6) in dimensionless form,

$$\hat{V} = \left[\frac{\hat{R}^2}{3} - \frac{\hat{r}^2}{2} \right] (\hat{R} + \varepsilon), \quad (8)$$

$$\hat{A} = \frac{1}{2} \hat{R}^2 \left[1 + \mathcal{F}(\hat{R}, \varepsilon) \right] - \frac{\hat{r}^2}{2}, \quad (9)$$

in which

$$\varepsilon = \hat{L} - \hat{R}, \quad (10)$$

and

$$\mathcal{F}(\hat{R}, \varepsilon) = \frac{(\hat{R} + \varepsilon)^2}{\hat{R} \sqrt{\varepsilon(2\hat{R} + \varepsilon)}} \arcsin \left(\frac{\sqrt{\varepsilon(2\hat{R} + \varepsilon)}}{\hat{R} + \varepsilon} \right). \quad (11)$$

Since $\varepsilon \ll 1$, $\mathcal{F}(\hat{R}, \varepsilon)$ may be expanded as a series near $\varepsilon = 0$,

$$\mathcal{F}(\hat{R}, \varepsilon) = 1 + \frac{4\varepsilon}{3\hat{R}} + O(\varepsilon^2). \quad (12)$$

Taking a derivative of (8) with respect to time, we neglect terms multiplying $d\varepsilon/dt$ (since $|d\varepsilon/dt| \ll |d\hat{R}/d\hat{t}|$; see Fig. 3b) to obtain

$$\frac{d\hat{V}}{d\hat{t}} = \left(\hat{R}^2 - \frac{\hat{r}^2}{2} + \frac{2\hat{R}\varepsilon}{3} \right) \frac{d\hat{R}}{d\hat{t}}. \quad (13)$$

Substituting Eq. (12) into Eq. (9) and using Eq. (13) we recover the result for a spherical droplet,

$$\hat{\Lambda} = \frac{d\hat{R}}{d\hat{t}} + O(\varepsilon^2), \quad (14)$$

for weakly-spheroidal droplets such as the ones in our experiments.

4.2. Empirical correlation

Linear regression to the data of $R(t)$ and $L(t)$ yields constant values for $\Lambda \approx dR/dt$ at varying X and DR . These Λ data are then fitted using the parameters measured in each experiment – pressure amplitude (p_1), velocity amplitude (u_1) and the phase-angle deviation from $\pi/2$, expected for a pure standing wave,

$$\theta = \phi - \pi/2, \quad (15)$$

where ϕ denotes the pressure-velocity phase lag. The temperature and humidity measurements varied negligibly throughout the experiments and hence were taken as constants. In dimensionless form, we may write $\Lambda/\Lambda_{NA} = f(Re, P, \theta)$, where Λ_{NA} marks the value measured in the absence of acoustics, $Re = |u_1|R/\nu$ is the Reynolds number, with $|u_1|$ the maximal droplet-gas relative velocity and ν the gas kinematic viscosity, and $P = |p_1|/p_m$. Previous studies on acoustic-driven droplet evaporation treated the acoustic field simply as a means for generating relative velocity between the droplet and gas, i.e. $\Lambda/\Lambda_{NA} = f(Re)$. In most studies, a standard power-law behavior of the form

$$\frac{\Lambda}{\Lambda_{NA}} = cRe^\alpha \quad (16)$$

is correlated to the data [7,21], where c, α are two free parameters that are set to optimize the data fitting. Here, we suggest a generalization to this approach, accounting for variations in P, θ . Since both P and θ can locally be zero without terminating the evaporation (for instance $P = 0$ at $X \approx 0.49$ in Fig. 4a), extending the regular power law behavior in the form $\Lambda \propto Re^\alpha P^\beta \theta^\gamma$ yields a non-physical result. Alternatively, we suggest the generalization

$$\frac{\Lambda}{\Lambda_{NA}} = cRe^{\alpha+\beta P+\gamma\theta}, \quad (17)$$

for which Eq. (16) is retrieved as a limiting case by setting $P = \theta = 0$. β and γ are the additional free parameters, physically rep-

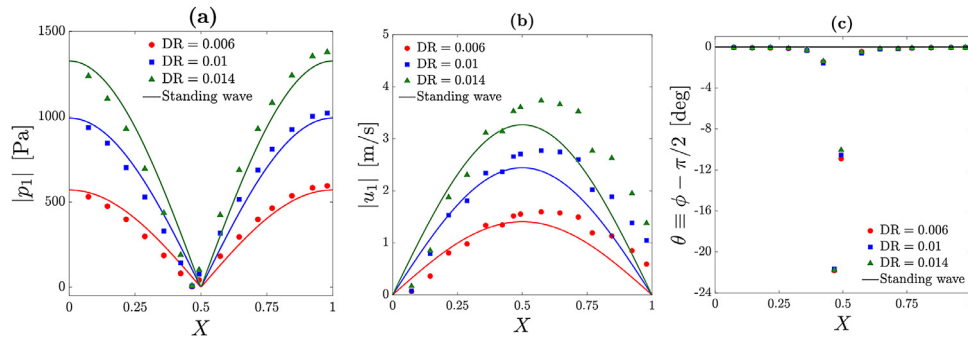


Fig. 4. The spatial distribution of (a) pressure oscillations, (b) velocity oscillations and (c) phase lag deviation from that of a pure standing wave, θ , for all DR. Lines represent a pure standing wave distribution and markers denote actual measurements. An increase in DR trivially increases p_1 and u_1 , however the results clearly indicate that θ is nearly independent of DR.

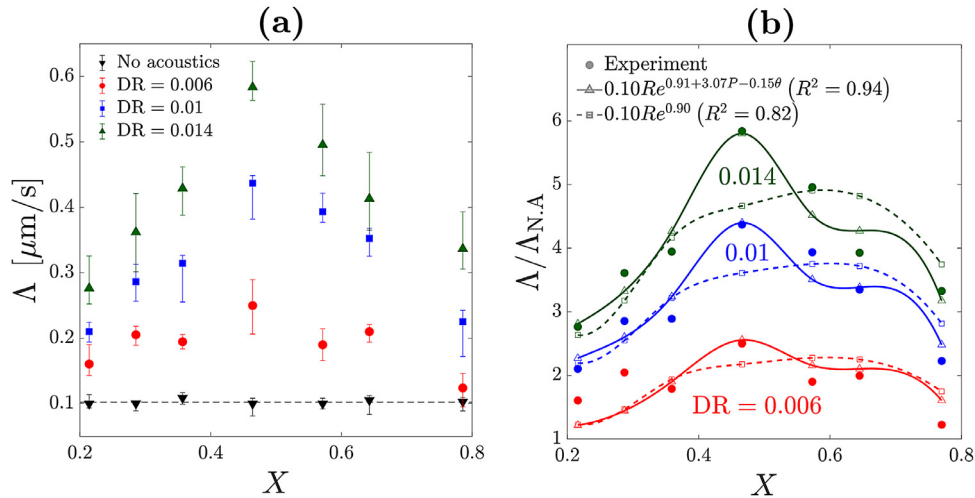


Fig. 5. Summary of the experiments conducted on the droplet evaporation at varying conditions: (a) Dimensional results of $\Lambda \approx dR/dt$, representing the droplet diminution rate, at seven positions along the resonator for all DR, as well as in the absence of acoustics. The dashed line marks the average of the 'no acoustics' measurements. The error bars mark the range of the measurements through three repetitions. (b) Dimensionless results - Filled circles denote the experimental data, scaled by its respective value with no acoustics; squares and triangles denote the optimal curve-fitting results for Eqs. (16) and (17), respectively. The solid and dashed lines are splines connecting between the triangles and squares, respectively, to visualize the trends of the correlations.

resenting the supplementary degrees of freedom that emerge from consideration of additional acoustic field characteristics besides the velocity.

Fig. 5 a presents the experimental measurements for Λ at varying X and DR (red circles, blue squares and up-facing triangles for DR = 0.006, 0.01, 0.014, respectively), including values with no acoustics (black down-facing triangles). Error bars denote the measurement range for three repetitions, and the dashed black line represents the mean of the no acoustics measurements. As expected, the evaporation in the absence of acoustics is nearly independent of position since no velocity is induced. As DR is increased, the evaporation rate trivially increases. In order to closely study the effect of the acoustic field features on the evaporation, we scale the results of DR = 0.006, 0.01, 0.014 with their respective 'no acoustics' counterparts, and present the dimensionless results (filled circles) in Fig. 5b. Values along the y axis then represent the evaporation rate multiplying factor by which the acoustics exceeds the quiescent base state. The squares and triangles represent the respective values for each experiment, calculated according to Eqs. 16-(17), respectively, with the constants indicated in the legend. These constants were obtained by regular minimum search for the optimal curve fitting to the experimental data. The dashed and solid lines are splines that connect between the values calculated through Eqs. 16-(17), respectively, so as to visualize the trend of the theoretical predictions.

An increase in DR increases both P and Re , and the evaporation rate, as expected, is naturally enhanced. The largest droplet diminution rate \forall DR is observed near the resonator center, where $|\theta|$ is maximized, $P \propto |p_1|$ is minimized and $Re \propto |u_1|$ nears its peak (see Fig. 4). As clearly seen, the standard power law correlation in Eq. (16) fails to describe the droplet evaporation rate near the resonator center and predicts a maximum at $X \approx 0.6$, where the velocity is largest, as seen in Fig. 4b. In reality, the highest evaporation rate was consistently measured at $X = 0.464$ - not where the velocity maximizes - such that fitting the data based solely on relative velocity between the droplet and gas cannot accurately explain the phenomenon. Moreover, a symmetry in $|u_1|$ about the maximal value yields similar Re at small and large X . Consequently, the standard power law correlation under and over-predicts the results at small and large X , respectively. The suggested generalization to Eq. (16), which accounts for variations in P and θ , significantly improves the predictions, increasing the fitting parameter from $R^2 = 0.82$ to $R^2 = 0.94$. In particular, it accurately recovers the maximal evaporation rates due to the abrupt increase in θ near the resonator center. The nearly identical values obtained for c and α when fitting the data with Eqs. 16-(17) validates that Eq. (17) is indeed a generalized version of Eq. (16), where the role of relative velocity in enhancing the evaporation rate remains unchanged. Interestingly, the maximum evaporation rates recorded at DR = 0.006, 0.01, 0.014 - $\Lambda/\Lambda_{NA} \approx 2.5, 4.3, 5.8$, respectively -

quantitatively match the respective maxima reported by Berdugo *et al.* [18] (Fig. 4a), who investigated the effect of acoustics on the evaporation rate of a droplet aerosol. This agreement suggests that the evaporation of a droplet collection in an acoustic field may be deduced by the elementary physics of a single droplet evaporation process in similar conditions.

5. Conclusion

We have demonstrated that acoustic-driven droplet evaporation differs from a simple oscillatory motion of gas over a droplet, and that the organic characteristics of an acoustic field – pressure, velocity and phase between them – all affect the evaporation rate. In particular, the phase angle between pressure and velocity was found to dramatically affect the evaporation rate, in our case enhancing the evaporation as the waveform deviates from that of a standing wave. These findings can dramatically impact the design of future devices for precise droplet evaporation, where an increase in $|\theta|$, which strongly correlates with an increase in the droplet evaporation rate, can be easily achieved through addition of passive flow obstruction elements that distort the acoustic wave and induce phasing between p_1 and u_1 . The suggested correlation, accounting for all the inherent acoustic features, quantitatively matches the experimental observations and may therefore be used for the design of such acoustic-driven droplet vaporizers.

Declaration of Competing Interest

The authors declare that they have no known competing financial interests or personal relationships that could have appeared to influence the work reported in this paper.

Supplementary material

Supplementary material associated with this article can be found, in the online version, at doi:[10.1016/j.ijheatmasstransfer.2021.121071](https://doi.org/10.1016/j.ijheatmasstransfer.2021.121071)

CRediT authorship contribution statement

Avshalom Offner: Methodology, Software, Data curation, Writing - original draft, Writing - review & editing, Visualization, Investigation, Formal analysis. **Nir Berdugo:** Conceptualization, Methodology, Software, Data curation, Writing - original draft, Writing - review & editing, Visualization, Investigation, Formal analysis. **Dan Liberzon:** Conceptualization, Methodology, Writing - original draft, Writing - review & editing, Investigation, Formal analysis, Supervision, Project administration.

References

- [1] E. Morteza, A. Mahmoud, A. Nasser, Modeling of solution droplet evaporation and particle evolution in droplet-to-particle spray methods, *Drying Technology* 27 (1) (2009) 3–13, doi:[10.1080/07373930802565665](https://doi.org/10.1080/07373930802565665).
- [2] M. Ordoubadi, F.K.A. Gregson, O. Melhem, D. Barona, R.E.H. Miles, D. D'Sa, S. Gracin, D. Lechuga-Ballesteros, J.P. Reid, W.H. Finlay, R. Vehring, Multi-solvent microdroplet evaporation: modeling and measurement of spray-drying kinetics with inhalable pharmaceuticals, *Pharmaceutical Research* 36 (2019) 100.
- [3] J.L. Garcia-Cordero, Z.H. Fan, Sessile droplets for chemical and biological assays, *Lab on a Chip* 17 (2017) 2150–2166.
- [4] Y.J.P. Carreón, M. Ríos-Ramírez, R.E. Moctezuma, J. González-Gutiérrez, Texture analysis of protein deposits produced by droplet evaporation, *Scientific Reports* 8 (2018) 9580.
- [5] O. Weltsch, A. Offner, D. Liberzon, G.Z. Ramon, Adsorption-mediated mass streaming in a standing acoustic wave, *Physical Review Letters* 118 (2017) 244301, doi:[10.1103/PhysRevLett.118.244301](https://doi.org/10.1103/PhysRevLett.118.244301).
- [6] Y. Blayer, N. Elkayam, G.Z. Ramon, Phase-dependence of sorption-induced mass streaming in an acoustic field, *Applied Physics Letters* 115 (3) (2019) 033703, doi:[10.1063/1.5110601](https://doi.org/10.1063/1.5110601).
- [7] A.P. Burdakov, V.E. Nakoryakov, On mass transfer in an acoustic field, *Journal of Applied Mechanics and Technical Physics* 2 (1965) 62–66, doi:[10.1007/BF00915612](https://doi.org/10.1007/BF00915612).
- [8] A.L. Yarin, G. Brenn, O. Kastner, D. Rensink, C. Tropea, Evaporation of acoustically levitated droplets, *Journal of Fluid Mechanics* 399 (1999) 151–204.
- [9] B. Ali Al Zaitone, C. Tropea, Evaporation of pure liquid droplets: Comparison of droplet evaporation in an acoustic field versus glass-filament, *Chemical Engineering Science* 66 (17) (2011) 3914–3921, doi:[10.1016/j.ces.2011.05.011](https://doi.org/10.1016/j.ces.2011.05.011).
- [10] Y. Niimura, K. Hasegawa, Evaporation of droplet in mid-air: Pure and binary droplets in single-axis acoustic levitator, *PloS one* 14 (2) (2019), doi:[10.1371/journal.pone.0212074](https://doi.org/10.1371/journal.pone.0212074). e0212074–e0212074
- [11] K. Kobayashi, A. Goda, K. Hasegawa, Y. Abe, Flow structure and evaporation behavior of an acoustically levitated droplet, *Physics of Fluids* 30 (8) (2018) 082105.
- [12] Y. Maruyama, K. Hasegawa, Evaporation and drying kinetics of water-nacl droplets via acoustic levitation, *RSC Adv.* 10 (2020) 1870–1877.
- [13] P.D. Richardson, Local effects of horizontal and vertical sound fields on natural convection from a horizontal cylinder, *Journal of Sound and Vibration* 10 (1) (1969) 32–41, doi:[10.1016/0022-460x\(69\)90127-8](https://doi.org/10.1016/0022-460x(69)90127-8).
- [14] A.M.A. Taweel, J. Landau, Mass transfer between solid spheres and oscillating fluids - A critical review, *The Canadian Journal of Chemical Engineering* 54 (1976) 532–539, doi:[10.1002/cjce.5450540530](https://doi.org/10.1002/cjce.5450540530).
- [15] P.S. Larsen, J.W. Jensen, Evaporation rates of drops in forced convection with superposed transverse sound field, *International Journal of Heat and Mass Transfer* 21 (4) (1978) 511–517, doi:[10.1016/0017-9310\(78\)90085-6](https://doi.org/10.1016/0017-9310(78)90085-6).
- [16] R.I. Sujith, G.A. Waldherr, J.I. Jagoda, B.T. Zinn, Experimental Investigation of the Evaporation of Droplets in Axial Acoustic Fields, *Journal of Vibration and Acoustics* 121 (3) (1999) 286–294, doi:[10.1115/1.2889722](https://doi.org/10.1115/1.2889722).
- [17] R.I. Sujith, G.A. Waldherr, J.I. Jagoda, B.T. Zinn, A Theoretical Investigation of the Behavior of Droplets in Axial Acoustic Fields, *Journal of Propulsion and Power* 16 (2) (2000) 278–285, doi:[10.2514/2.5566](https://doi.org/10.2514/2.5566).
- [18] N. Berdugo, M. Stolar, D. Liberzon, Enhancement of water droplet evaporation rate by application of low frequency acoustic field, *International Journal of Multiphase Flow* 126 (2020) 103217, doi:[10.1016/j.ijmultiphaseflow.2020.103217](https://doi.org/10.1016/j.ijmultiphaseflow.2020.103217).
- [19] A.M. Fusco, W.C. Ward, G.W. Swift, Two-sensor power measurements in lossy ducts, *Journal of the Acoustical Society of America* 91 (4) (1992) 2229–2235, doi:[10.1121/1.403656](https://doi.org/10.1121/1.403656).
- [20] D.B. Spalding, Theory of particle combustion at high pressures, *ARS Journal* 29 (1959) 828–835.
- [21] W.R. Ranz W.E. Marshall Evaporation from drops part I, *Chemical Engineering Progress* 48, 1952.